International Journal of Heat and Mass Transfer 119 (2018) 117–127

Contents lists available at ScienceDirect

International Journal of Heat and Mass Transfer

journal homepage: www.elsevier.com/locate/ijhmt

Convective heat transfer of a rotating multi-stage cavity with axial throughflow

Yongkai Quan, Di Han, Guoqiang Xu, Jie Wen *, Xiang Luo

National Key Lab. of Science and Technology on Aero-thermodynamics, School of Energy and Power Engineering, Beihang University, Beijing 100191, China

ARTICLE INFO

Article history:
Received 12 July 2017
Received in revised form 23 October 2017
Accepted 20 November 2017
Available online 25 November 2017

Keywords:
Multi-stage cavity
Axial throughflow
Heat transfer coefficient (HTC)
HTC sensor

ABSTRACT

The heat transfer characteristics in an engine-like rotating multi-stage cavity with axial throughflow are experimentally investigated. The cavity is a model of high pressure compressor in gas turbine, which has a gap ratio of 0.24 and a radius ratio of 0.23. Herein, the effects of inertial force, centrifugal buoyancy force, Coriolis force on the heat transfer coefficient (HTC) and the surface temperature distribution are analyzed and discussed. The heat transfer coefficient is measured with an innovative HTC sensor whereas the surface temperature is measured by embedded thermocouples when the shroud is heated by an induction heater. The measurements are conducted in a wide range of non-dimensional parameters: the maximum axial Reynolds numbers, rotational Reynolds numbers and buoyancy parameter can reach 9.87×10^4, 1.81×10^6 and 0.3, respectively. According to the experimental results, two regions with significantly different heat transfer characteristics could be identified on both side of the interested disc, namely, the forced convection zone caused by impingement cooling in the low radius area, and the Rayleigh-Bénard-like convection zone in the medium and high radius areas. On both windward and leeward sides of the disc, the heat transfer coefficients are zigzagging along the radial direction with two observed peak values.

1. Introduction

In modern aircraft gas turbines, the compressed air is sucked from the compressor to cool the high temperature components, such as the combustors; turbines and bearings. The bled cooling air then has to travel through the discs of high pressure compressors to reach the cooling site. However, the cavities between the compressor discs can generate the significant secondary flows, which give rise to the resulting convective heat transfer between the cooling air and the discs. Therefore, it is necessary to know the temperature distribution and heat transfer characteristics of the compressor discs since they influence the temperature of the cooling air as well as the thermal stress of the rotating discs. The convective heat transfer in rotating cavities has been widely investigated. The three dimensional unsteady flow inside the rotational cavities attracts many research attentions due to its complexity and importance. Both flow and heat transfer related investigations have been conducted.

1.1. Flow structure

It is recognized that the flow structure in the cavity with axial throughflow depends strongly not only on the surface temperature distribution but also on the geometric parameters. Farthing et al. [1] made flow visualization and velocity measurements under isothermal and non-isothermal conditions in the study of a simplified model for the flow that occurs between adjacent corotating compressor discs. Isothermal tests were conducted over a series of gap ratios with $0.133 < G=s/b < 0.533$. For a gap ratio of $G = 0.24$, which corresponded to this study, the axial throughflow of air created two toroidal vortices, one on top of the other (Fig. 1a). Reducing the gap ratio G (or Rossby number Ro) resulted in a weaker vortex. However, once the heated flow was involved, the flow structure was significantly different, and it was no longer axisymmetric. Both cyclonic and anti-cyclonic circulations were observed in the cavity. The cold air entered the cavity through a so-called "radial arm" (Fig. 1b). The low pressure of cyclonic circulation and the high pressure of anti-cyclonic circulation led to the pressure variations in the circumferential direction. The resulting pressure gradient provided the Coriolis force for the radial flow of fluid between two discs. Different from the heated disc, when the shroud was heated, the multiple "radial arms" could be observed [2]. More than single-stage cavities, Long et al. [3]

* Corresponding author.
E-mail addresses: quanyongkai@buaa.edu.cn (Y. Quan), handi@buaa.edu.cn (D. Han), guoqiang_xu@buaa.edu.cn (G. Xu), wenjie@buaa.edu.cn (J. Wen), xiang.luo@buaa.edu.cn (X. Luo).

https://doi.org/10.1016/j.ijheatmasstransfer.2017.11.110
0017-9310/

Nomenclature

A	heat transfer area [m^2]
a	inner radius of cavity [m]
b	outer radius of cavity [m]
r	radial coordinate [m]
s	axial space between discs [m]
m	mass flow [kg/s]
T	temperature [K]
G	gap ratio [=s/b]
X	nondimensional radius [=r/b]
Gr	generic Grashof number $\left[=\frac{\beta\rho_0^2\omega_0^2(T_{sh}-T_0)b^4}{\mu_0^2}\right]$
h (HTC)	heat transfer coefficient [w/(m^2·K)]
Nu	Nusselt number [=hb/λ_0]
Ro	Rossby number [=$W_0/(\Omega \cdot b)$]
Re_z	axial Reynolds number $\left[=\frac{2\rho_0 W_0 a}{\mu_0}\right]$
Re_ω	rotational Reynolds number $\left[=\frac{\rho_0\omega_0 b^2}{\mu_0}\right]$
β	volume expansion coefficient 1/k $\left[=\frac{1}{T_0}\right]$
ΔT_{max}	maximum temperature difference k [=$T_{sh}-T_0$]
Φ	heat power
λ	thermal conductivity [w/(m·K)]
μ	dynamic viscosity [kg/(m·s)]
ρ	density [kg/m^3]
Ω	angular speed [rad/s]

Subscripts

0	mainstream parameters
max	maximum
Sh	Shroud
f	reference value
w	wall
net	net value
loss	heat loss
ses	value of the sensor
std	value of the calibration
ave	average value

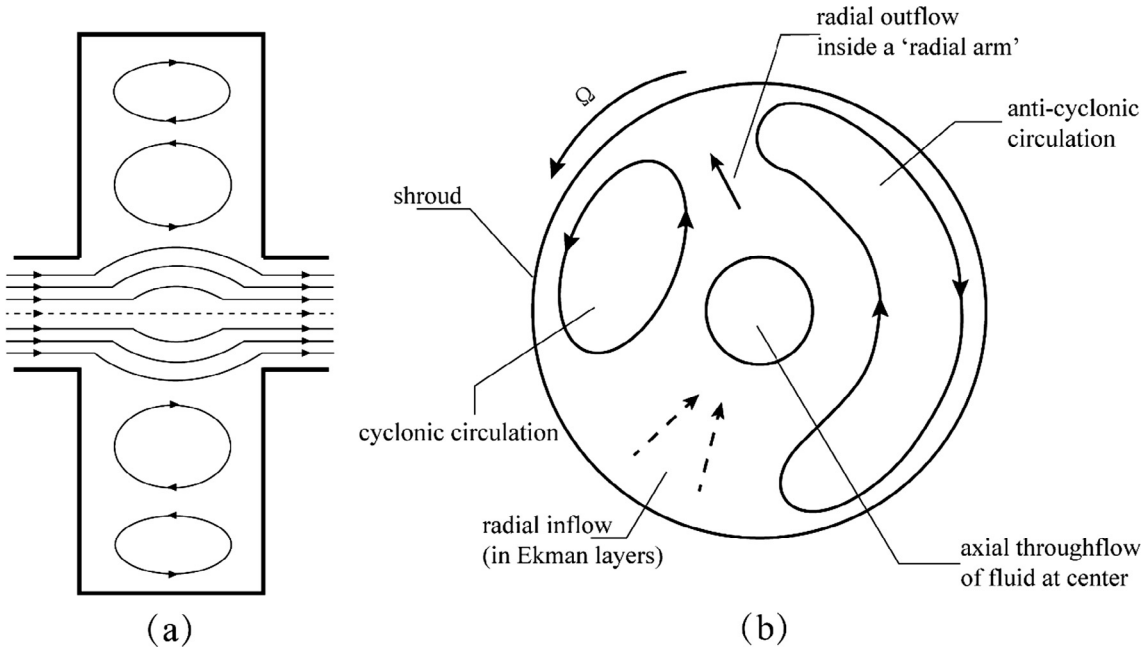

Fig. 1. Flow structures for an isothermal cavity (r-z-plane, a) and a heated rotating cavity (r-θ-plane, b).

conducted the flow visualization inside a heated multiple rotating cavity with axial throughflow. The velocities inside the cavities were in accord with the flow structure consisting of pairs of contra rotating vortices.

Buoyancy-induced flow occurs in the cavities when the temperature of the discs and shroud is higher than that of the air in the cavities. Owen et al. [4] focused on the effects of buoyancy force on the flow structure. The results showed that the velocity field was three dimensional and highly unsteady due to the buoyancy force. Moreover, the buoyancy-induced flow could be described by the Ekman-layer equations, in which only the core flow and the Ekman-layer were focused on [5]. Besides, Owen et al. [6] had studied the buoyancy-induced flow occurred in the rotating cavities with the principles of far-from-equilibrium thermodynamics. These thermodynamic concepts could be used to explain how many vortex pairs are formed in the rotating cavities. As mentioned above, the buoyancy could drive the instable flows in the rotating cavities [7,8]. The results indicated that two regions with distinct characteristics could be identified: a free convection in the high radius area and a forced convection in the low radius area. The higher rotational Reynolds number or Grashof number resulted in the lesser vortices, the stronger free convection, the weaker forced convection and vice versa.

1.2. Heat transfer

The convective heat transfer in the rotating cavities majorly depended on the flow parameters such as Re_z, Re_ω, Gr as well as the temperature distribution of the rotating disc. Farthing et al. [9] compared the heat transfer on the discs with the positive or

negative temperature gradient in radial-outward direction. The Nusselt numbers depended on the disc temperature distribution significantly. Luo et al. [10] discussed the effects of Re_z and Re_ω on the local heat transfer in a rotor-stator cavity with an inlet at the low radius location. The heat transfer coefficient measured with the transient thermochromic liquid crystal (TLC) technique was mainly influenced by the rotational Reynolds number (Re_ω) and the flow rate coefficient. Besides, Tang et al. [11] used the fin equation to calculate the Nusselt numbers of rotating discs based on the temperature data measured by Atkins and Kanjirakkad [12]. Furthermore, Tang et al. [13] developed a theoretical model to predict the Nusselt numbers and the temperature profiles on the compressor disc based on the fin equation. The theoretical distributions of Nusselt numbers and disc temperature agreed well with the experimental results, especially at the higher Grashof numbers when the buoyancy-induced flow dominated.

The buoyancy effects on the heat transfer in rotating cavities with axial throughflow have been well studied by researchers. Owen and Powell [4] measured the Nusselt numbers in a heated rotating cavity when the values of Re_ω was up to 3.2×10^6 and Re_z up to 4.8×10^4. The heat transfer on the disc was influenced significantly by the buoyancy force when the values of Re_z was small. While the larger Re_z, resulted in an increase in the heat transfer at the low radius area, which was similar with the effects of the axial throughflow of cooling air dominating the flow. It was reported that the free convection was the dominate factor when the momentum of the axial flow was low or the buoyancy force was strong [14,15]. The buoyancy-induced flow instability strengthened the convection in the cavity whereas the axial throughflow elevated the flow mixing or depressed the vortexes. Both of them resulted in a higher heat transfer of the rotating discs [16]. More details about the buoyancy-induced flow in rotating cavities could be seen in the review of Owen and Long [17].

1.3. Heat transfer measurements techniques

In order to measure the heat transfer coefficient of the heated shroud or rotating discs, fluxmeters or thermocouples were commonly used in the previous mentioned literatures. In addition, Newton et al. and Owen et al. [18,19] employed thermochromic liquid crystal (TLC) technique for the measurements of "slow transient" cases and made an improvement of the transient TLC technique. According to their results, experimenters could quantify and minimise the uncertainties in HTC resulting from the use of narrow-band TLC in slow-transient heat-transfer experiments. Such as the application to a rotating disc, Lock et al. [20] and Luo et al. [21,22] analyzed the convective heat transfer of a simplified model of a gas turbine rotor–stator system and added to the lack of available experimental data concerning the heat transfer characteristics. Also, the convective heat transfer on the rotating disc was investigated by Pellé and Harmand [23,24] with infrared thermography technique. Based on the surface temperature measured with this technique, a new thermal balance equation was used to identify the local heat transfer coefficient. Uffrecht et al. [25] developed an electro-thermal measurement system to measure the heat transfer coefficients in gaseous flow with metallic boundaries. It provided a new determination of the fluid reference temperature and delivered always positive heat transfer coefficients. What is more, the miniaturized HTC sensors with low energy consumption fulfilled the requirements of the turbomachinery measurements [26].

As mentioned above, the flow parameters such as Re_z, Re_ω, Gr as well as the disc temperature distribution are critical important in influencing the flow and heat transfer in the rotating cavities. However, most investigations employed the single-stage cavities and the simplified geometries as the model, which were different from the real engine. Besides, aside from a variety of traditional heat transfer measurements techniques in the rotating discs, and new methods were kept developing and testing in the literatures. Therefore, the objective of this work is to investigate the heat transfer in an engine-like multi-stage rotating cavities with a novel HTC measurements technique.

2. Experimental investigation

2.1. Test rig

As shown in Fig. 2, the experiments are conducted on a rotating platform. The system consists of the air supply subsystem, the heating subsystem, the test section and the data acquisition subsystem. The rotating components are driven by a 30 KW thyristor-controlled electric motor and the maximum rotational speed, which is measured (to an accuracy of ±1 rpm) with an tacho-ratiometer, is 3000 rpm. The mass flow of the cooling air is measured with a FCI-ST98 Thermal Flowmeter, and the uncertainty is about ±3%. The voltage outputs of the temperature and HTC sensors are converted into digital data with an AD-converter module, and then the digital data are transmitted to a computer using the slip-rings. The pressurized air enters the rotating hollow shaft, flows through the discrete holes to rectify the air, and then reaches the test section.

The test section (Fig. 3) includes five stainless steel discs (four cavities). The temperature and the heat transfer measurements are performed on the third stage disc, and the associated second cavity has a gap ratio of $G = 0.24$ and a radius ratio of $a/b = 0.23$. There are a series of thermocouples and heat transfer coefficient sensors on the windward and leeward surface of the rotating discs. The surface temperature of the discs and air inlet temperature are measured by the 0.3 mm (in diameter) T-type (copper-constantan) thermocouples. The uncertainty of the thermocouple measurements was calibrated to be ±0.3 °C/100 °C. The beads of the thermocouples are welded on the metal surface. Then the wires of thermocouples and the HTC sensors are covered by stainless steel sheets in order to avoid the flow disturbance. The HTC measurements are introduced in the next section in detail. The locations of the thermocouples and heat transfer coefficient sensors are shown in Table 1. The disc shroud is heated by an induction heater with a maximum heating power of 7 KW. The experimental parameters and the uncertainties are summarized in Table 2.

2.2. Heat transfer coefficient measurements

The convective heat transfer coefficient is an important index to evaluate the strength of the wall-to-fluid thermal energy transfer. Traditionally, the local and the average heat transfer coefficients are calculated based on the Laplace's equation and Newton's law of cooling according to the boundary conditions measured by thermocouples [27,28]. The HTC calculated by this method is negative in some locations. Besides, this approach is an example of an inverse problem where small uncertainties in the temperatures could create large uncertainties in the computed heat transfer coefficients [29]. In this work, we employed a new method, which has been developed and validated by Quan et al. [30], to measure the heat transfer coefficient with a small HTC sensor. The HTC sensor is a cylinder with diameter of $D = 10$ mm and height of $H = 7$ mm. It includes heating plate, thermocouples, shell of the body and adiabatic dope as shown in Fig. 4(a). The heating plate, which is the key component, is made of lacquered wire winding ($d = 0.06$ mm) with double layer. The advantages of the heating plate are: uniform heat flux and convenience for adding electric field. To reduce radiant heat loss, the heating plate is covered with

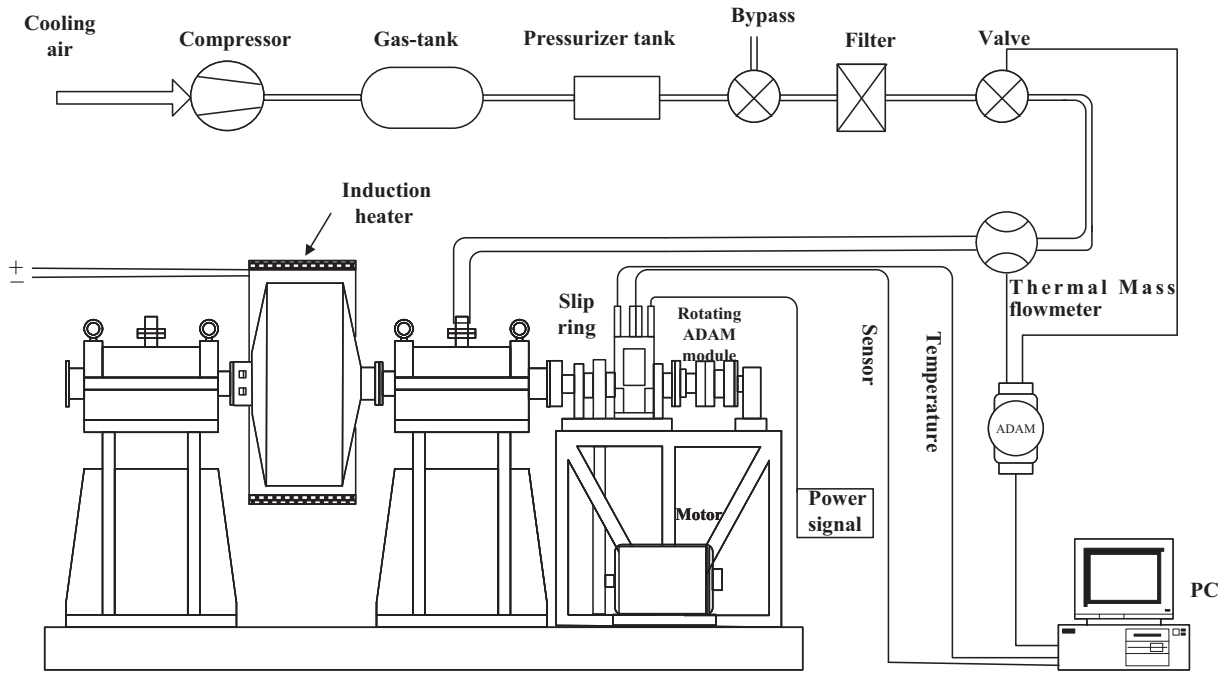

Fig. 2. Scheme diagram of the rotating test rig.

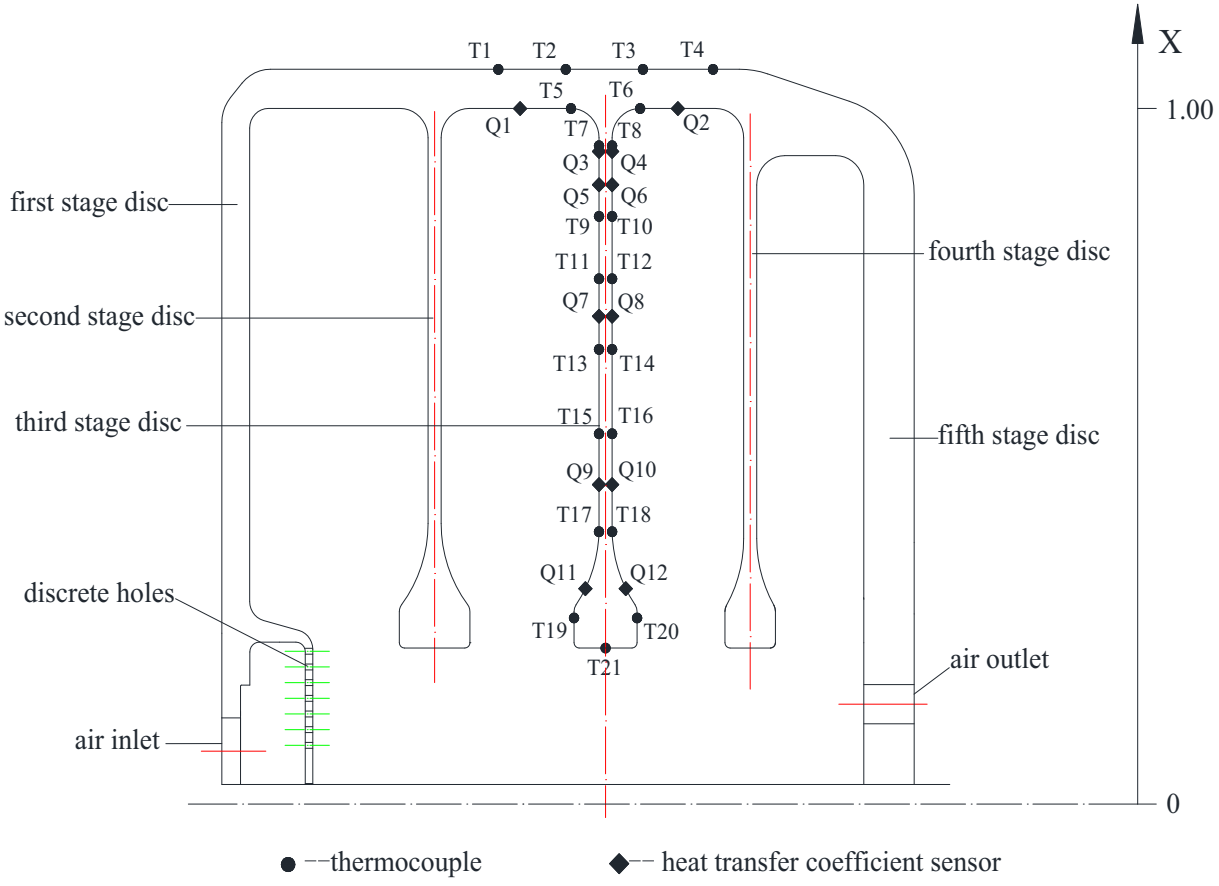

Fig. 3. Scheme diagram of the multiple-cavity test section.

Table 1
Radial locations of thermocouples and heat transfer coefficient sensors.

The locations of the thermocouples		The locations of the heat transfer coefficient sensors	
Number	$X = r/b$	Number	$X = r/b$
T1–T4	1.056	Q1(Q2)	1
T5(T6)	1	Q3(Q4)	0.938
T7(T8)	0.946	Q5(Q6)	0.89
T9(T10)	0.845	Q7(Q8)	0.701
T11(T12)	0.755	Q9(Q10)	0.46
T13(T14)	0.654	Q11(Q12)	0.31
T15(T16)	0.532		
T17(T18)	0.392		
T19(T20)	0.268		
T21	0.225		

Table 2
Experimental parameters and uncertainties.

Parameters	Range	Uncertainty
ω (rad/s)	$62.8 \leqq \omega \leqq 209.4$	±1 rad/s
m (kg/s)	$0.08 \leqq m \leqq 0.22$	±3%
T_{sh}	$333 \leqq T_{sh} \leqq 373$	±0.3 K
Re_ω	$5.42 \times 10^5 \leqq Re_\omega \leqq 1.81 \times 10^6$	0.07–0.18%
Re_z	$3.73 \times 10^4 \leqq Re_z \leqq 9.87 \times 10^4$	1.93–5.04%
$\beta\Delta T_{max}$	$0.16 \leqq \beta\Delta T_{max} \leqq 0.3$	1–1.86%

an aluminum foil. The shell is made of polyfluortetraethylene and the insulations are used to reduce the conductive heat loss in radial and axial direction. According to the Newton's law of cooling, the heat transfer coefficient, h, could be calculated as follows.

$$h = \frac{\Phi_{net}}{A(T_w - T_f)} = (UI - \Phi_{loss})/A(T_w - T_f) \quad (1)$$

where Φ_{net} is the net heat power, A is the heat transfer area on the heating plate, T_w is the temperature of the heating plate which is measured by the thermocouple 1 and T_f is the fluid inlet temperature. The total heat power of the heating plate is determined by the voltage U and the current I. The heat loss (Φ_{loss}) is calculated based on the temperature difference ΔT between the thermocouple 1 and 2 as shown in Fig. 4(a). In order to calibrate the relation between the heat loss and the temperature difference, a separated heat loss calibration experiment is conducted, in which the front surface of the sensor is covered with the insulation (in this case, $h = 0$ and therefore $UI = \Phi_{loss}$). A fitting relationship between the ΔT and the heat loss (Φ_{loss}) is obtained by changing the heating power (which equals to Φ_{loss}). When applying the sensors, the modified heat loss could be calculated by submitting the real temperature difference ΔT to Eq. (2).

$$\Phi_{loss} = UI = F(\Delta T) \quad (2)$$

The calibrations of the HTC sensors are conducted under both non-rotating and rotating conditions. Firstly, the HTC sensors are installed in a non-rotating rectangular pipe, as shown in Fig. 4(b) which has an inner diameter of 0.048 m and a length of 4 m. The distance between the sensor and the inlet of the pipe is 3.5 m where the flow has been fully developed. Aside from the HTC sensors, the calibration apparatus as shown in Fig. 4c (a carbon film heater with a thickness of 0.2 mm) is installed in the channel to measure an average heat transfer coefficient as the reference. The carbon film is the key component whose role is similar to the heating plate of the HTC sensors. Different from the HTC sensors, the thermal insulation of the calibration apparatus is better with the effects of the large-area polystyrene board (the cross-sectional dimensions: 320 × 80 mm, thickness: 100 mm). Therefore, the calibration apparatus can use the Eq. (1) to obtain the HTC which is more accurate. Moreover, two heat transfer correlations are compared with the results of the calibration apparatus in the Appendix A. The calibration results of the HTC sensor under the constant inlet Reynolds number are shown in Fig. 5(a). There is a good repeatability although the temperature difference ΔT between the thermocouple 1 and 2 is different. However, heat transfer coefficients measured by the sensors are not equal to the calculated HTC with the calibration apparatus. Therefore, a correlation factor K, which is the ratio between the heat transfer coefficient measured by the sensor and that measured by the calibration apparatus, is introduced as $K = h_{ses}/h_{std}$. Fig. 5(b) shows that the

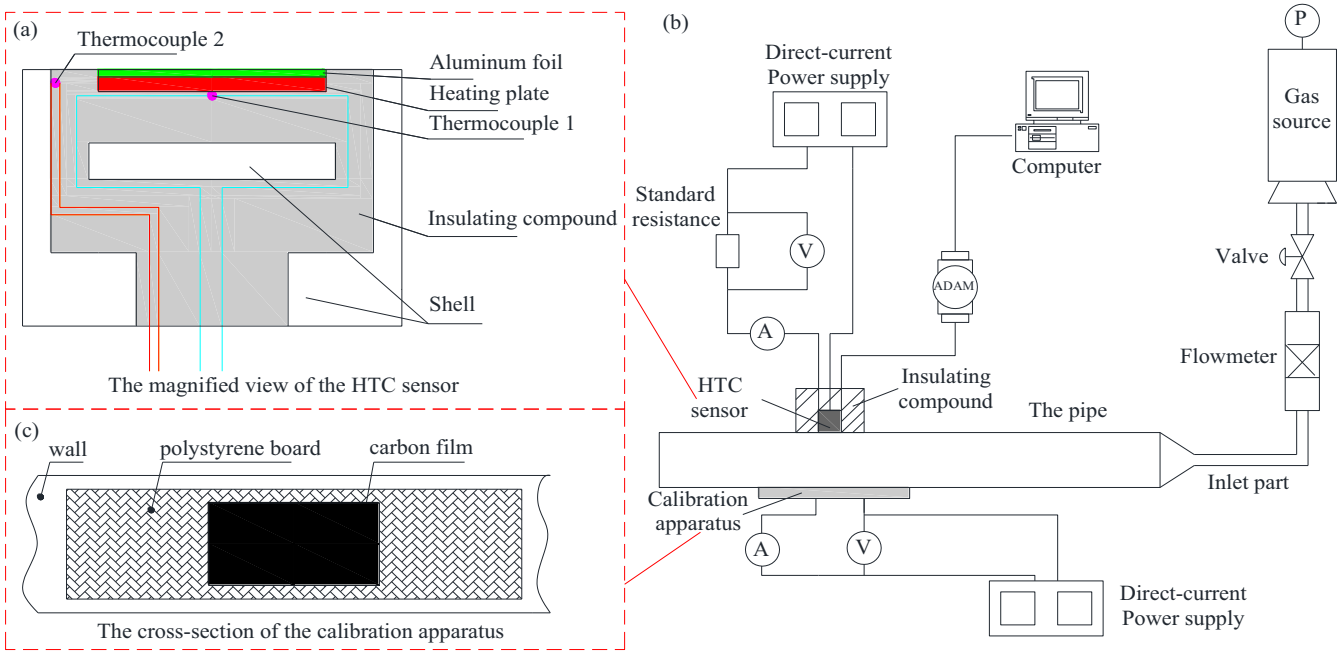

Fig. 4. (a) The magnified view of the HTC sensor. (b) Schematic diagram of the non-rotating calibration system. (c) The cross-section of the calibration apparatus.

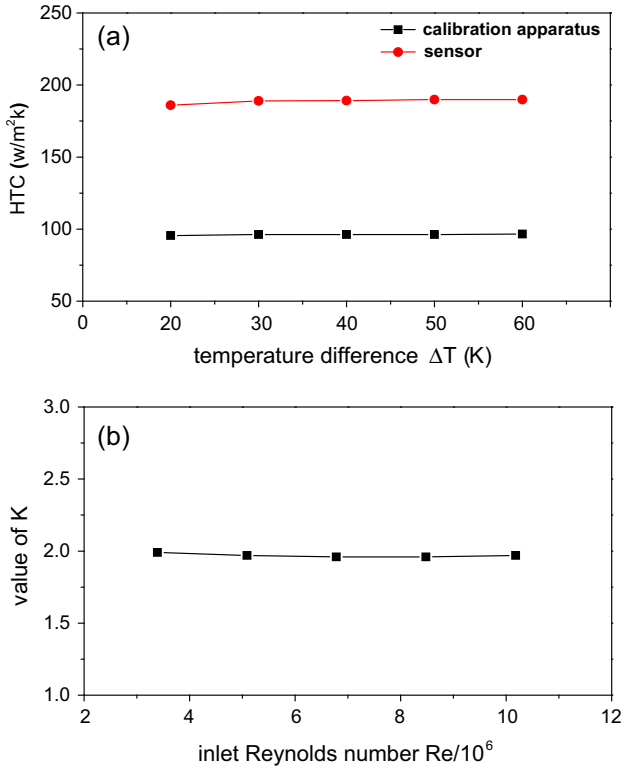

Fig. 5. (a) Temperature characteristic of the HTC sensor (inlet Reynolds number $Re = 6.78 \times 10^6$). (b) Correlation factor of K versus the inlet Reynolds number.

correlation factor K is kept at a constant of around 1.97 for a variety of inlet Reynolds numbers. Secondly, the sensors are assembled on a rotating stainless steel disc with a diameter of 800 mm and a thickness of 25 mm, the sensor is installed at the location with the radius 250 mm. In both cases, the outputs of the sensors are compared with the calibration apparatus in each configuration, and the results show that the K has the same value under non-rotating and rotating state. It is calibrated that the relative uncertainty of the HTC measurements is less than 5%. Besides, artificial factors have important influence on the manufacture of the sensors, so different sensor has different value of K.

3. Experimental results and analysis

In a rotating cavity, the flow and heat transfer is normally influenced by the following factors: the momentum of the axial flow, the rotation induced Coriolis force, and the rotation induced buoyancy. Therefore, the effects of Re_z, Re_ω, and $\beta\Delta T_{max}$ are investigated and discussed individually.

The local temperature and HTC distributions presented below could be better explained by flow models given by the previous research of Farthing et al. [1] and Long et al. [3] described in the introduction. Previous research by Owen et al. [4] showed that the flow inside heated rotating cavities is three-dimensional and unsteady, especially the effects of buoyancy-induced vortex structures in the r-θ-plane, seen in Fig. 1(b). The assumed, time-averaged flow structures for the investigated flow cases are shown in Fig. 6. A flow structure in the r-z-plane with two toroidal vortices is assumed, corresponding to flow visualizations by Farthing et al. [1] shown in the Fig.1(a) as a result of the supposed radial symmetry and the time-averaging at thermal steady state conditions.

3.1. The effect of the inertia force of the axial flow

In order to investigate the effect of Re_z on the wall temperature distribution, the rotational Reynolds numbers and the buoyancy parameter $\beta\Delta T$ are fixed at 9.03×10^5 and 0.23, respectively.

The temperature distributions on the windward and leeward surface are not identical as shown in Fig. 7. The temperature on the windward surface decreases when the Re_z, which represents the effect of inertia force, increases from 3.73×10^4 to 9.87×10^4. Besides, the temperature changes significantly (about 27.92% at $X = 0.268$) in the low radius area which is mainly impacted by the axial throughflow, this is because the increase of inertia force could strengthen the forced convection and heat transfer. In the high radius area ($X = 0.946$), the temperature variation is only about 7.61%. The reason could be inferred that the free convection is dominant in the high radius area due to limited axial throughflow. Our temperature distributions are in agreement with the results of the theoretical model of Owen et al. [13], for a given value of Gr, the values of the Nusselt numbers decreased as Re_z decreased, which caused an increase in the temperature of the disc.

Fig. 8 compares the variations of the average temperature in the low radius area of windward surface and leeward surface. Here, T_{ave} is the average of the temperature at the location of $X = 0.225$, 0.268 and 0.392. In general, the average temperature on the leeward surface is higher than that on the windward surface, and the temperature drop is smaller with the higher Re_z. It indicates that the influence of inertia force on the heat transfer on windward surface is more significant. Moreover, the difference between the average temperatures on the two surfaces is enlarged with an increase in Re_z. The possible explanations are proposed as follows. First, a small fraction of the axial throughflow flows into the second cavity and cools the windward surface. Once it mixes with the mainstream, the flow temperature at the downstream locations, such as in the third cavity, increases which results in a decrease of the local convective heat transfer on the leeward surface. Second, the windward surface is prone to be effected by the axial throughflow induced impingement, whereas the leeward surface is majorly influenced by the backflow. Therefore, a more significant influence is observed on the windward surface.

The radial variations of heat transfer coefficients on windward and leeward surfaces, as shown in Fig. 9, are significantly non-symmetrical. On the windward surface, the HTC is zigzagging in the radial direction, and two peaks could be identified (see Fig. 9 (a)). The first peak appears at the higher radius $X = 0.46$ instead of the lowest radius area (the border of central wheel rim and disc) on the disc due to the impingement effect of the axial flow. There is a location ($X = 0.701$) of the local minimum of the HTC due to the border between the inner and outer vortices. Then, owing to the direction of the rotation of the outer vortex, cold air impinges in this area and the HTC increases there (from $X = 0.701$ to $X = 0.89$). So, the second peak appears at $X = 0.89$, which should be induced by the highly unsteady flow around the outer vortex. The heat transfer coefficients at the first three points (X<=0.701) increase significantly with an increase in Re_z (see Fig. 9(b)). The most significant heat transfer enhancement (about 36.05% from $Re_z = 3.73 \times 10^4$ to $Re_z = 9.87 \times 10^4$) is observed at the location of $X = 0.46$ where the first peak is measured. It supports our previous assumption that the inertia force plays more significant role in influencing the heat transfer in the low radius area. This is also consistent with the findings of Owen et al. [4] who found that the effects were consistent with the circulation created by the cooling air dominating over the buoyancy-induced flow.

On the leeward surface, as shown in Fig. 9(c), an apparent difference can be distinguished. Firstly, the point with the lowest radius presents the highest heat transfer in the forced convection zone (among the first three points). Then, it decreases in the

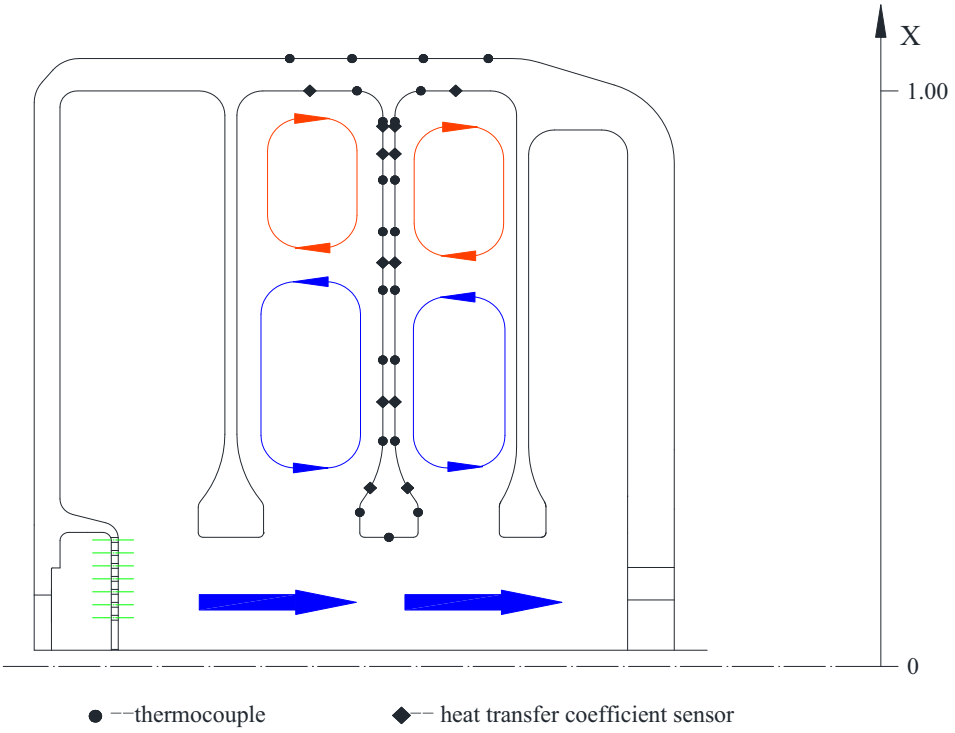

Fig. 6. Assumed time-averaged flow structures inside two rotating cavities.

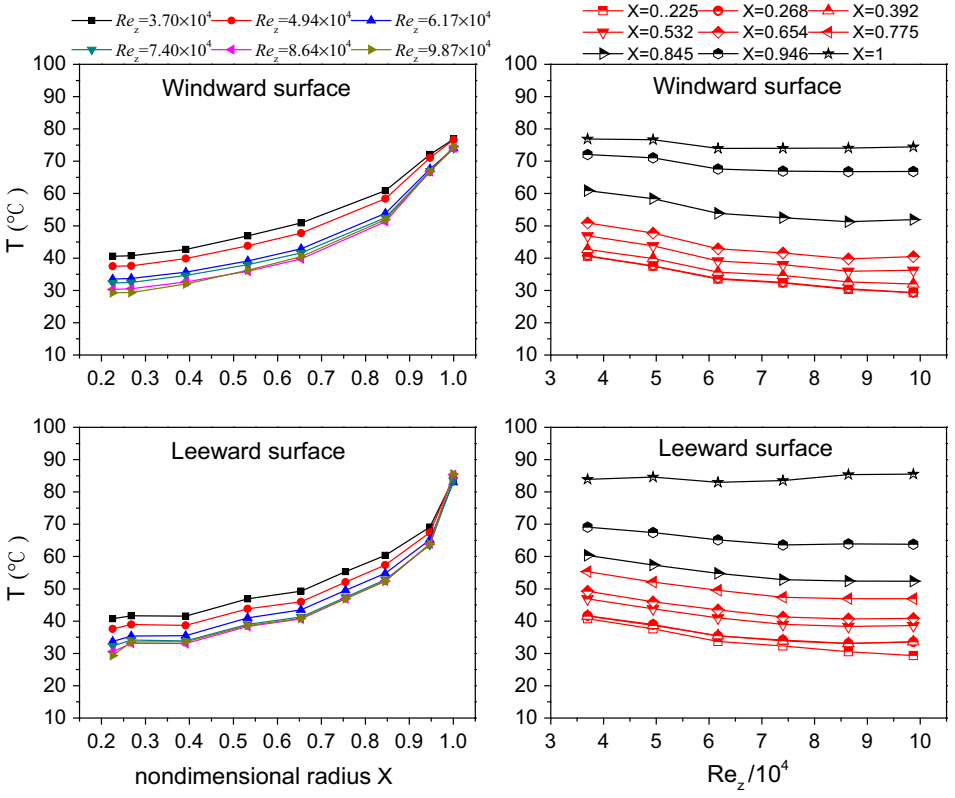

Fig. 7. The temperature distributions on the disc when $\beta\Delta T_{max} = 0.23$ and $Re_\omega = 9.03 \times 10^5$.

radial-outward direction. In general, the heat transfer coefficients are smaller than that on the windward counterparts. Besides, the most significant heat transfer increase is found on the first point ($X = 0.31$), and it increases by about 31.82% when the axial Reynolds number changes from $Re_z = 3.73 \times 10^4$ to $Re_z = 9.87 \times 10^4$ (see Fig. 9(d)). The reason could be inferred as follows. The axial

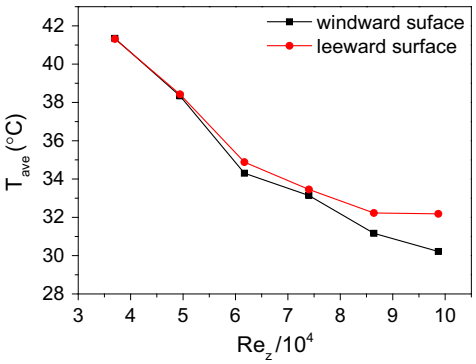

Fig. 8. Effects of Re_z on the average temperature in the low radius area.

flow generates vortexes after traveling through the center hole of the rotating disc. The area with the lower radius is closer to the strong inner vortex, and therefore, has the higher heat transfer.

In general, the HTC and the axial heat flux can evaluate the strength of the wall-to-fluid thermal energy transfer for thermal steady-state measurement. It is interesting to find that our radial distributions of the HTC are in consistent with the axial heat flux measured by Günther et al. [31] with a two-cavity teat rig (the gap ratio of $G = 0.27$ and the radius ratio of $a/b = 0.21$). Both of the radial distributions are zigzag and there are two peak values along the radial direction, one at smaller radius and the other at larger radius, especially on the windward surface. Between the two peaks, there is a location ($X = 0.701$) of the local minimum of the HTC due to the border between the inner and outer vortices as shown in Fig. 6. By comparing the location of the minimum, it can be found that the result of Günther et al. [31] seems to be $X = 0.65$ for different flow cases. Besides, the measurement by Patounas et al. [32] in a test rig with real engine components shows the locations of the "turning-points" in the same region ($X = 0.7$). However, different from the previous investigations, the two peak values are our research focus. Further investigations to clarify these turning-points should be done.

On both windward and leeward surfaces, the cavity could be separated into two parts in radial direction based on the heat transfer measurements. In the low radius area ($X \leq 0.701$), the effect of Re_z is significant whereas the axial flow rate plays little role in the high radius area ($X > 0.701$). The results agree well with the previous investigations [3,7], in which the flow in the heated rotating cavity is a mixture of the forced convection and the Rayleigh-Bénard-like convection in the centrifugal force field if the temperature gradient shares the same direction with the centrifugal acceleration, therefore, different heat transfer characteristics are observed in the two zones.

3.2. The effect of centrifugal buoyancy force

Compared to the non-rotating cavity, the rotation influences the flow and heat transfer by two different means: disturb the flow in a non-heated cavity and generate the buoyancy field in a heated cavity. In order to separate the two effects, the rotational effect on the non-heated cavity is firstly investigated. Then the effect of buoyancy is analyzed in the heated cavity.

As mentioned, two peaks of heat transfer are observed on each surface. The following analysis focuses on the locations where the peak values are observed. Fig. 10 shows the effect of rotational Reynolds number on the heat transfer at those four points. In

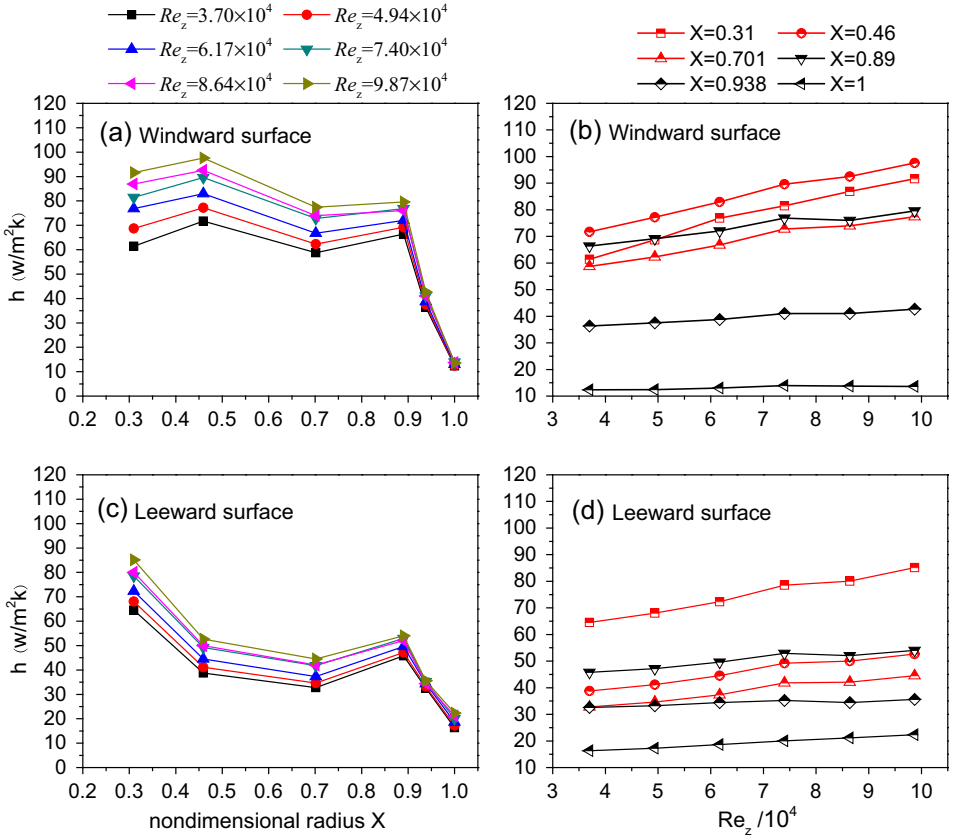

Fig. 9. (a, c) The radial distributions of the HTC and (b, d) Effects of Re_z on the HTC when $\beta\Delta T_{max} = 0.23$ and $Re_\omega = 1.35 \times 10^6$.

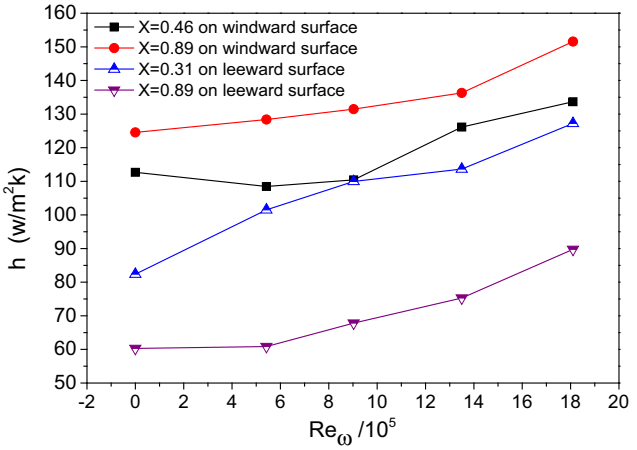

Fig. 10. Effects of Re_{ω} on the peak values of HTC when $\beta\Delta T_{max} \approx 0$ and $Re_z = 4.94 \times 10^4$.

general, the heat transfer is enhanced by the rotation on every points. The most significant enhancement (around 21.69%) is observed on the point of $X = 0.89$, windward surface. It is higher than the heat transfer on the low radius peak instead of the previous case which is higher in low radius shown in Fig. 9(a). The reasons could be inferred as follows: the rotation breaks the vortices and promotes the mixing of the axial flow and the cavity flow, therefore, elevates the heat transfer in general.

The above measurements and analysis are performed in an isothermal disc whose temperature is equal to the inlet temperature of cooling air, where the buoyancy plays no role. However, in the real application, the buoyancy force influences the flow and heat transfer due to the large temperature gradient. Therefore, it is interesting to investigate the effect of the buoyancy in the cavity. The strength of the buoyancy is normally described by the buoyancy parameter of the fluid ($\beta\Delta T_{max}$). In order to investigate the effect of Centrifugal buoyancy force on the convective heat transfer, the rotational and the axial Reynolds numbers are kept at constants. As shown in Fig. 11, the heat transfer significantly

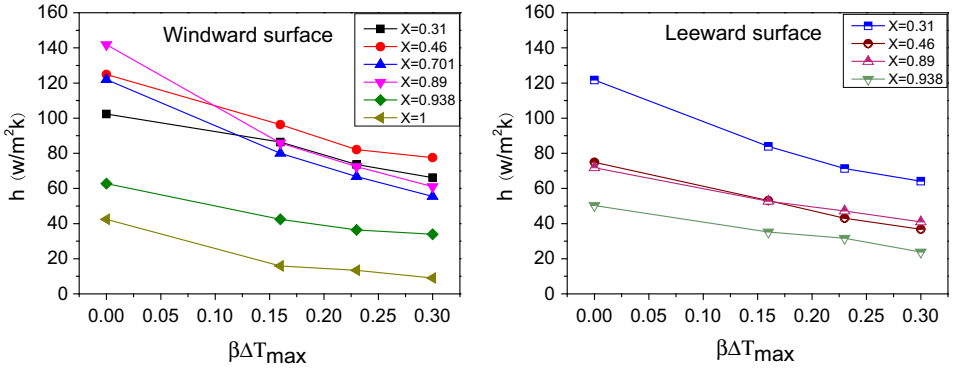

Fig. 11. Effects of $\beta\Delta T_{max}$ on HTC variations when $Re_{\omega} = 9.03 \times 10^5$ and $Re_z = 6.17 \times 10^4$.

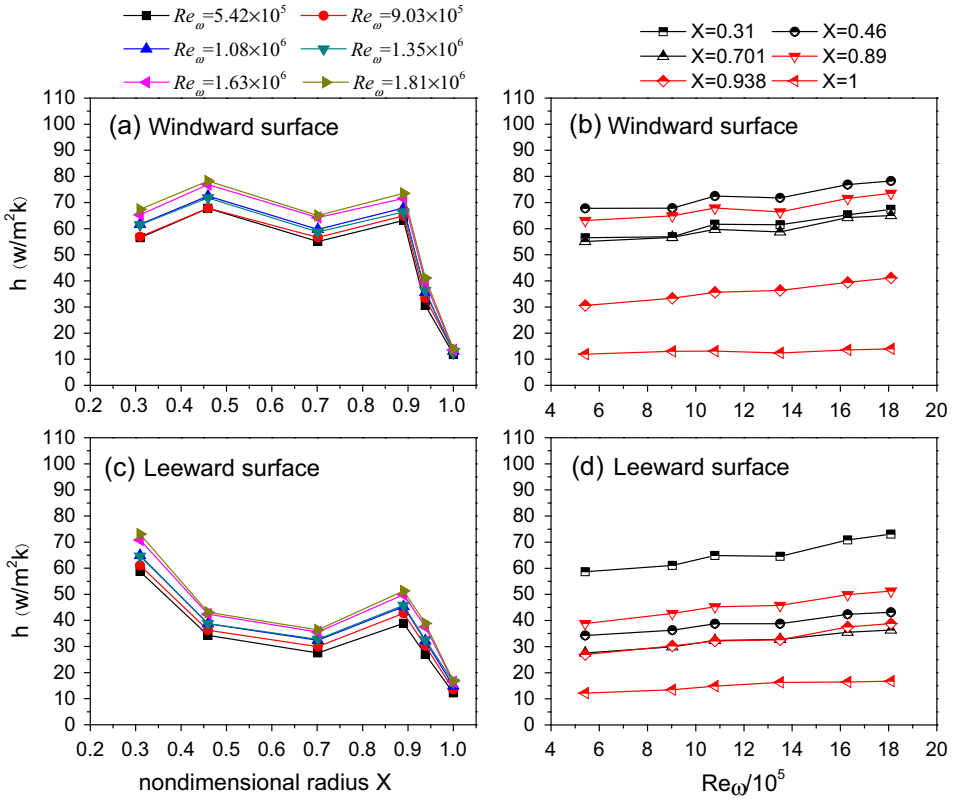

Fig. 12. (a, c) The radial distributions of the HTC and (b, d) Effects of Re_{ω} on the HTC when $\beta\Delta T_{max} = 0.23$, $Re_z = 3.7 \times 10^4$.

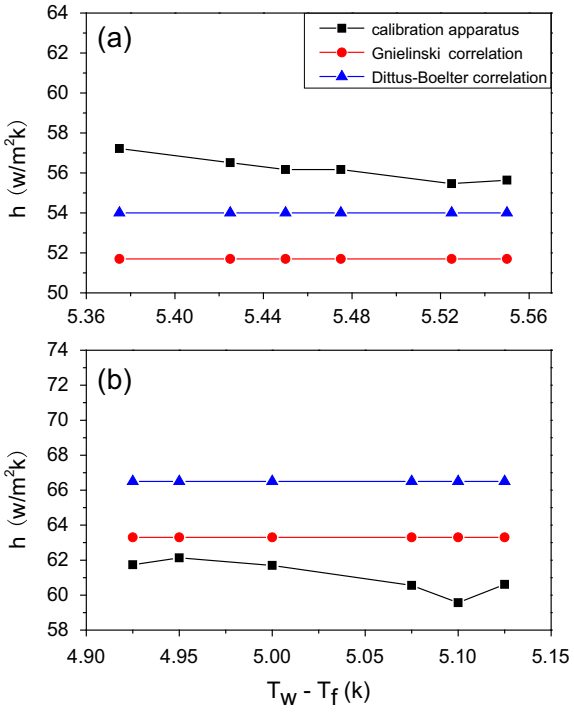

Fig. 13. The comparison with the heat transfer correlations. (a) $Re = 4.34 \times 10^4$, (b) $Re = 5.66 \times 10^4$.

decreases while the buoyancy parameter increases. The most obvious HTC decrease is measured as 56.98% at $X = 0.89$. The study of TIAN [7] turned out that the free convection dominated the flow in the cavity as Centrifugal buoyancy force increased. However, the enhancement of the free convection made it difficult for cooling air to flow to high radius area. As a result, the heat transfer in high radius area decreased.

3.3. The effects of the Coriolis force and centrifugal buoyancy force

In this section, the axial Reynolds number and the buoyancy parameter are fixed at $Re_z = 3.7 \times 10^4$ and $\beta\Delta T_{max} = 0.23$ separately. As shown in Fig. 12(a), the overall heat transfer coefficients increase with an increase in Re_ω. A significant heat transfer increase is observed in the high radius area, for example, the heat transfer is enhanced by about 34.35% at the location $X = 0.938$ on the windward surface when the rotational Reynold number increases from $Re_\omega = 5.42 \times 10^5$ to $Re_\omega = 1.81 \times 10^6$ (shown in Fig. 12b). Besides, the two peak values are approximately equal instead of the previous case shown in Fig. 9(a) which is bigger in low radius and smaller in high radius with increasing axial Reynolds number. Given that the inertia force of the axial flow is mainly influencing the low radius area, the heat transfer in the high radius area is largely affected by the Coriolis force and centrifugal buoyancy force. Meanwhile, centrifugal buoyancy force strengthens the Rayleigh-Bénard-like convection and weakens the forced convection. In the low radius area, the heat transfer is affected in two different ways. On one hand, the Coriolis force enhances the flow mixing, and in turn elevates the heat transfer. On the other hand, the increase of the mass fraction of the axial flow, which is sucked into the cavity, results in a weaker impingement effect and a lower heat transfer rate. As a result, the heat transfer in the low radius area has a modest increase with an increase in rotational Reynolds numbers.

In general, the heat transfer on the leeward surface is lower than the windward side (Fig. 12c). The heat transfer in the low radius area ($X = 0.46$) increases by about 25.87% (Fig. 12d) when Re_ω increases from 5.42×10^5 to 1.81×10^6, whereas the heat transfer coefficient increases by about 43.83% at $X = 0.938$ in the medium and high radius areas. The reasons could be inferred as follows: the heat transfer in the medium and high radius areas is affected by two mechanism. On one hand, the area dominated by the Rayleigh-Bénard-like convection expands. Therefore, the enhancement of the medium and high radius areas is more significant. On the other hand, the increase of the mass flow which flows into the cavity causes the flow field of this area more disorderly.

4. Conclusions

The heat transfer in an engine-like multi-stage rotating discs is investigated. Based on the measured heat transfer coefficient and surface temperature distributions, two different regimes could be identified: the forced convection zone caused by the impingement of axial flow in the low radius area and the Rayleigh-Bénard-like convection zone in the medium and high radius areas. On both windward and leeward surfaces, the heat transfer coefficients are zigzagging along the radial direction. The two peaks are located in the forced convection zone and the Rayleigh-Bénard-like convection zone, respectively. However, different from the windward surface, the peak value which is located at the forced convection zone on the leeward surface appears at the lowest radius area on the disc and is smaller than that on the windward surface.

The inertial force of the axial flow mainly influences the flow and heat transfer in the low radius area of the cavity and the effect on the windward surface is greater than the leeward side. The disc surface temperature decreases with an increase in Re_z (i.e. inertial force). Also, the two peak values of the heat transfer coefficients increase, especially the one located in the forced convection zone.

The Coriolis force and the centrifugal buoyancy force mainly influence the heat transfer in the medium and high radius areas. The Rayleigh-Bénard-like convection and heat transfer in the medium and high radius areas are significantly enhanced with an increase in Re_ω. However, the heat transfer in the low radius area is slightly influenced by them.

Conflict of interest

The authors declared that there is no conflict of interest.

Appendix A

As shown in Fig. 13, the results of the calibration apparatus are compared with the Dittus-Boelter and Gnielinski correlations when the Reynolds numbers are 4.34×10^4 and 5.66×10^4. The empirical correlations are obtained based on experiments under special experimental conditions. Compared with the correlations, the HTC measured with the calibration apparatus has a certain error due to the different experimental conditions. The limits of the experimental error are 4.6–8.5% compared with the Gnielinski correlations and 2.8–6.0% compared with the Dittus-Boelter correlations when the Reynolds numbers is 4.34×10^4. While when the Reynolds numbers is 5.66×10^4, the limits of the experimental error are 2.5–5.9% compared with the Gnielinski correlations and 7.5–8.9% compared with the Dittus-Boelter correlations.

References

[1] P.R. Farthing, C.A. Long, J.M. Owen, J.R. Pincombe, Rotating cavity with axial throughflow of cooling air – flow structure, J. Turbomach. 114 (1) (1990) 229–236.
[2] R.P. Farthing, The Effect of Geometry on Flow and Heat Transfer in a Rotating Cavity, University of Sussex, 1988.

[3] C.A. Long, N.D.D. Miché, P.R.N. Childs, Flow measurements inside a heated multiple rotating cavity with axial throughflow, Int. J. Heat Fluid Flow 28 (6) (2007) 1391–1404.
[4] J.M. Owen, J. Powell, Buoyancy-induced flow in a heated rotating cavity, J. Eng. Gas Turbines Power 128 (1) (2004) 341–347.
[5] J.M. Owen, H. Tang, Theoretical model of buoyancy-induced flow in rotating cavities, J. Turbomach. 137 (11) (2015).
[6] J.M. Owen, Thermodynamic analysis of buoyancy-induced flow in rotating cavities, J. Turbomach. 132 (3) (2010) 1149–1158.
[7] S. Tian, Z. Tao, S. Ding, G. Xu, Computation of buoyancy-induced flow in a heated rotating cavity with an axial throughflow of cooling air, Int. J. Heat Mass Transf. 51 (3) (2008) 960–968.
[8] S.J.M. Habraken, G. Nienhuis, Rotational stabilization and destabilization of an optical cavity, Phys. Rev. A 79 (1) (2008) 11662.
[9] P.R. Farthing, C.A. Long, J.M. Owen, J.R. Pincombe, Rotating cavity with axial throughflow of cooling air – heat transfer, J. Turbomach. 114 (1) (1990) 229–236.
[10] X. Luo, X. Zhao, L. Wang, H. Wu, G. Xu, Flow structure and heat transfer characteristics in rotor–stator cavity with inlet at low radius, Appl. Therm. Eng. 70 (1) (2014) 291–306.
[11] H. Tang, T. Shardlow, J.M. Owen, Use of fin equation to calculate nusselt numbers for rotating discs, J. Turbomach. 137 (12) (2015).
[12] N.R. Atkins, V. Kanjirakkad, Flow in a Rotating Cavity with Axial Throughflow at Engine Representative Conditions, 2014.
[13] H. Tang, J. Michael Owen, Effect of buoyancy-induced rotating flow on temperatures of compressor disks, J. Eng. Gas Turbines Power 139 (6) (2017), 062506-062506-062510.
[14] J.M. Owen, E.D. Bilimoria, Heat transfer in rotating cylindrical cavities, J. Mech. Eng. Sci. 19 (4) (1977) 175–187.
[15] J.M. Owen, H.S. Onur, Convective heat transfer in a rotating cylindrical cavity, Asme Trans. J. Eng. Power 105 (105) (1983) 265–271.
[16] C.A. Long, Disk heat transfer in a rotating cavity with an axial throughflow of cooling air, Int. J. Heat Fluid Flow 15 (4) (1994) 307–316.
[17] J.M. Owen, C.A. Long, Review of buoyancy-induced flow in rotating cavities, J. Turbomach. 137 (11) (2015).
[18] P.J. Newton, Y. Yan, N.E. Stevens, S.T. Evatt, G.D. Lock, J.M. Owen, Transient heat transfer measurements using thermochromic liquid crystal. Part 1: An improved technique, Int. J. Heat Fluid Flow 24 (1) (2003) 14–22.
[19] J.M. Owen, P.J. Newton, G.D. Lock, Transient heat transfer measurements using thermochromic liquid crystal. Part 2: Experimental uncertainties, Int. J. Heat Fluid Flow 24 (1) (2003) 23–28.
[20] G.D. Lock, Y. Yan, P.J. Newton, M. Wilson, J.M. Owen, Heat transfer measurements using liquid crystals in a preswirl rotating-disk system, J. Eng. Gas Turbines Power 127 (2) (2005) 935–944.
[21] X. Luo, L. Wang, X. Zhao, G. Xu, H. Wu, Experimental investigation of heat transfer in a rotor–stator cavity with cooling air inlet at low radius, Int. J. Heat Mass Transf. 76 (2014) 65–80.
[22] X. Luo, G. Han, H. Wu, L. Wang, G. Xu, Experimental investigation of pressure loss and heat transfer in a rotor–stator cavity with two outlets, Int. J. Heat Mass Transf. 78 (2014) 311–320.
[23] J. Pellé, S. Harmand, Heat transfer measurements in an opened rotor–stator system air-gap, Exp. Therm Fluid Sci. 31 (3) (2007) 165–180.
[24] J. Pellé, S. Harmand, Heat transfer study in a rotor–stator system air-gap with an axial inflow, Appl. Therm. Eng. 29 (8–9) (2009) 1532–1543.
[25] W. Uffrecht, A. Günther, V. Caspary, Electro-Thermal Measurement of Heat Transfer Coefficients, in: ASME Turbo Expo 2012: Turbine Technical Conference and Exposition, 2012.
[26] B. Heinschke, W. Uffrecht, A. Günther, S. Odenbach, V. Caspary, Telemetric Measurement of Heat Transfer Coefficients in Gaseous Flow: First Test of a Recent Sensor Concept in a Rotating Application, vol. 42, no. 6–7, 2014, pp. V006T006A015.
[27] A. Alexiou, N.J. Hills, C.A. Long, A.B. Turner, J.A. Millward, Heat transfer in high-pressure compressor gas turbine internal air systems: a rotating disc-cone cavity with axial throughflow, Exp. Heat Transfer 13 (4) (2000) 299–328.
[28] C. Long, P. Childs, The effect of inlet conditions on the flow and heat transfer in multiple rotating cavity with axial throughflow, J. Aerospace Power 22 (5) (2007) 683–693.
[29] J.M. Owen, On the computation of heat-transfer coefficients from imperfect temperature measurements, J. Magn. Reson. 165 (2) (2003) 230–236.
[30] Yong-kai Quan, Guo-qiang Xu, Xiang Luo Zhang, Development and calibration of heat transfer coefficient sensor for rotational state, J. Aerospace Power 26 (12) (2011) 2684–2690.
[31] A. Günther, W. Uffrecht, S. Odenbach, Local measurements of disc heat transfer in heated rotating cavities for several flow regimes, J. Turbomach. 134 (5) (2010) 991–1000.
[32] D.S. Patounas, C.A. Long, P.R.N. Childs, Disc Heat Transfer in Gas Turbine Compressor Internal Air Systems, 2009.